

Enhancement Mask for Hippocampus Detection and Segmentation

Dengsheng Chen, Wenxi Liu, You Huang, Yuanlong Yu
College of Mathematics and Computer Science
Fuzhou University

Tong Tong
Imperial Vision

Abstract—Detection and segmentation of the hippocampal structures in volumetric brain images is a challenging problem in the area of medical imaging. In this paper, we propose a two-stage 3D fully convolutional neural network that efficiently detects and segments the hippocampal structures. In particular, our approach first localizes the hippocampus from the whole volumetric image while obtaining a proposal for a rough segmentation. After localization, we apply the proposal as an enhancement mask to extract the fine structure of the hippocampus. The proposed method has been evaluated on a public dataset and compares with state-of-the-art approaches. Results indicate the effectiveness of the proposed method, which yields mean Dice Similarity Coefficients (i.e. DSC) of 0.897 and 0.900 for the left and right hippocampus, respectively. Furthermore, extensive experiments manifest that the proposed enhancement mask layer has remarkable benefits for accelerating training process and obtaining more accurate segmentation results.

Index Terms—3D Convolutional Neural Network, Fully Convolutional Neural Network, Hippocampus segmentation

I. INTRODUCTION

With pervasive applications of medical imaging, biological structure detection and segmentation have been fundamental and crucial tasks in biomedical imaging research. It extracts different tissues, organs, pathologies and biological structures, to support medical diagnosis surgical planning and treatments. In practice, the detection and segmentation are performed manually by pathologists, which is time-consuming and tedious. The ever-increasing variety of medical images make manual segmentation impracticable in terms of cost and reproducibility. Thus, automatic biomedical detection and segmentation are highly desirable. However, this task is extremely challenging, because of the heterogeneous of biological objects including the large variability in location, size, shape and frequency, and also because of low contrast, noise and other imaging artifacts caused by various medical imaging modalities and techniques [1].

In the past years, substantial progress has been made in biomedical image detection and segmentation with pixel-based methods [2]–[5] and structure-based methods [6]–[9]. In recent years, the fully convolutional networks (FCNs [10]), have been used for biomedical image segmentation, which require little hand-crafted features or prior knowledge. FCNs trained end-to-end have been previously applied to 2D images both in computer vision [11] and microscopy

image analysis [12]. These models are trained to predict a segmentation mask, delineating the structures of interest, for the whole image. Ronneberger et al. [12] proposed U-Net, a deep convolutional network that adds skip connections to the symmetric feature maps to perform 2D medical image segmentation. With data augmentation, it achieves significant improvement over previous methods. Recently, this approach was extended to 3D and applied to segmentation of volumetric data acquired from a confocal microscope [13]. With the inspiration of these models, Fausto et al. [1] divided model into stages that learn residuals and as empirically observed improve both results and convergence time. However, due to the heavy computational burden of 3D convolutional operation and a large number of uncertain parameters, it is formidable to devise an extremely deeper 3D neural network which inherits more hidden features. Furthermore, with the limitation of hardware devices, the prior methods have to downsample the high resolution medical image before feeding into networks, which gives rise to the loss of segmentation accuracy.

To handle the problems mentioned above, we present a novel two-stage 3D fully convolutional neural network, for detecting and segmenting biomedical objects from volumetric medical images, e.g. MRI. Our approach not only reduces the computational burden of 3D FCN, but also preserve the segmentation details. In particular, our model first learns the localization and segmentation context of the biomedical objects from the low resolution input and then integrate it with the original input by an enhancement mask that performs the fine structure segmentation. We experiment the proposed approach in a hippocampus segmentation dataset (ADNI) and achieve state-of-the-art results.

Main Contributions: We present a two-stage 3D fully convolutional neural network that efficiently detects and then segments the hippocampal structure from volumetric brain images. Our framework first learns the holistic structural information from the downsampled input image, which localizes the hippocampus, while roughly estimating the segmentation through a proposal network. In the second stage, we introduce an enhancement mask that integrates the rough segmentation proposal in a segmentation network to perform fine segmentation.

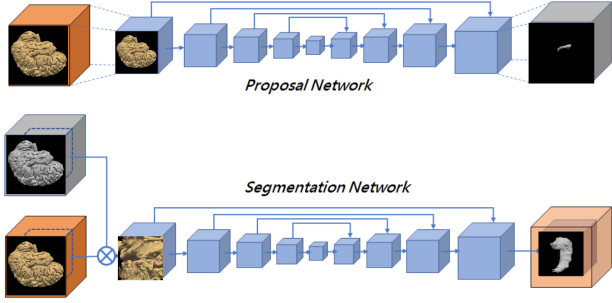


Fig. 1

OUR FRAMEWORK CONSISTS OF TWO-STAGE NETWORKS. IN THE FIRST STAGE, THE INPUT DATA (I.E. THE ORANGE CUBE) IS DOWNSAMPLED AND FED INTO A 3D FULLY CONVOLUTIONAL NEURAL NETWORK, CALLED *Proposal Network* WHICH LEARNS A HOLISTIC PROBABILITY MAP. AN ENHANCEMENT MASK WILL BE GENERATED FROM THIS PROBABILITY MAP. THE ENHANCEMENT MASK WILL BE APPLIED TO THE ORIGINAL DATA. WE WILL CROP A $64 \times 64 \times 64$ CUBE ACCORDING TO HIPPOCAMPUS LOCALIZATION FROM THE ENHANCEMENT DATA AS THE INPUT OF *Segmentation Network*. HENCE, THE SEGMENTATION NETWORK OUTPUTS THE FINE SEGMENTATION RESULT OF THE CROPPED DATA.

II. THE PROPOSED METHOD

In this paper, we propose a two-stage framework to detect the hippocampus from the volumetric brain images and then apply segmentation to the enhanced original image data through the enhancement mask layer. Our proposed framework can fully exploit the holistic information of the volumetric data and also efficiently perform the segmentation while preserving the fine structure of the hippocampus. Specifically, in the first stage (*Proposal Network*), the hippocampus is localized from the downsampled input volumetric data while a rough segmentation proposal of the hippocampus is learned with a 3D FCN. In the second stage (*Segmentation Network*), the original input data is enhanced through the enhancement mask which generates from *Proposal Network* and then cropped. We will introduce these two stages in the following subsections.

A. Proposal Network and Localizing Hippocampus

In our application, each image consists of several slices with the resolution of 256×256 (pixels) and the numbers of slices range from 166 to 256. Processing the original volumetric data requires a large amount of memory on the runtime. However, the holistic view of the volumetric data provide the crucial context to localize and segment the hippocampus. To fully exploit the holistic information of the input volumetric data, we build up *Proposal Network* to estimate the segmentation of the hippocampus. The architecture of *Proposal Network* is an encoder-decoder, which learns a probability map about pixelwise. As shown in Fig.1, *Proposal*

Network first compress the input data via multiple convolutional layers into feature maps with smaller resolutions, and then perform decompression by upsampling the feature maps layer-by-layer via de-convolution and combining with corresponding compressed feature maps respectively by skip-connection. The output of the network is the response of the segmented hippocampus which performs the pixelwise estimation on whether it belongs to the hippocampus.

To learn the holistic information, the original input data \mathbf{X} is downsampled to $64 \times 64 \times 128$ and fed into *Proposal Network* \mathcal{F} . At the end, the output response map is upsampled to the original size using 3D bilinear interpolation sampling technique. The whole procedure is denoted as $\mathcal{F}(\mathbf{X}) \in \mathbb{R}^{W \times H \times D}$. Intuitively, in the proposal network, learning the segmentation response from the downsampled low-resolution data actually enlarges the receptive field to cover the entire volumetric image. Although the accuracy of the segmentation at this stage is not satisfactory, the output response provides the crucial context for localizing the hippocampus whose volume is much smaller compared to the whole brain, and the rough segmentation results still make a vital improvement on further image segmentation through the enhancement mask which is generated from itself. Furthermore, since the whole image data is fed into *Proposal Network*, it makes the detection can be extended to other segmentation problems.

Localizing Hippocampus Before the segmentation, we need to localize the hippocampus in advance. In essence, the proposal response $\mathcal{F}(\mathbf{X})$ indicates the probability of whether the hippocampus shows up in each voxel. We denote it as $\mathbf{L}_{proposal}$ for clarity. The goal is to calculate the central coordinate of the hippocampus from $\mathbf{L}_{proposal}$. Instead of using sliding window or clustering, we accumulate the voxel value of $\mathbf{L}_{proposal}$ which is a tensor with the size of $W \times H \times D$ along the X, Y, and Z axis respectively. Taking the X axis for instance, the accumulation is computed as follows: $\mathbf{H}_X(i) = \sum_{j=1}^H \sum_{k=1}^D \mathbf{L}_{proposal}(i, j, k), \forall i \in [1, W]$. If $\mathbf{H}_X(i)$ is larger than a certain threshold ϵ , it indicates the occurrence of the hippocampus at the i^{th} slice along the X axis. Empirically, we set ϵ as 5 and it can effectively and efficiently filter out the false alarm in $\mathbf{L}_{proposal}$. Hence, we can compute the boundary coordinates by:

$$X_{min} = \arg \min_i \mathbf{H}_X(i), \quad (1)$$

$$X_{max} = \arg \max_i \mathbf{H}_X(i)$$

$$Y_{min} = \arg \min_i \mathbf{H}_Y(i),$$

$$Y_{max} = \arg \max_i \mathbf{H}_Y(i)$$

$$Z_{min} = \arg \min_i \mathbf{H}_Z(i),$$

$$Z_{max} = \arg \max_i \mathbf{H}_Z(i)$$

$$s.t. \mathbf{H}_X(i) > \epsilon, \mathbf{H}_Y(i) > \epsilon, \mathbf{H}_Z(i) > \epsilon \quad (2)$$

The central coordinate of localizing the hippocampus

is computed: $\mathbf{V}_{center} = \{(X_{max} + X_{min})/2, (Y_{max} + Y_{min})/2, (Z_{max} + Z_{min})/2\}$, where $X_{max}, X_{min}, Y_{max}, Y_{min}, Z_{max}, Z_{min}$ are the maximum and minimum coordinates along all axes.

B. Enhancement Mask Layer and Segmentation Network

Enhancement Mask Layer The enhancement mask \mathbf{M} is generated from the rough segmentation results of *Proposal Network* by the following formulation:

$$\mathbf{M} = \mathbf{L}_{proposal} * \alpha + \beta \quad (3)$$

where the $\mathbf{L}_{proposal}$ contains the holistic and reliable information which regard to the location of the hippocampus, but the details of its 3D structure is blurred due to resizing which needs to be compensated by the original data $\mathbf{C}_{original}$. Both α, β are the parameters which control the influence of the enhancement mask on the original image data. It is obviously that the bigger α and smaller β will cause a stronger influence of enhancement mask. As for $\mathbf{L}_{proposal}$ is 0/1 label value, we set β as 1 which respect for that we do not apply any enhance or suppress operation on the original background image data. The value of α is relatively flexible, and different α value will cause a significant different performance on the segmentation networks. A detail analysis on how to select a suitable α value will be shown in next section.

Segmentation Network In order to preserve the detailed structure of the hippocampus in segmentation, it is common practice to empirically crop a portion of voxels from the original volumetric image and then infer the segmentation based on this cropped volume. Although such cropping operation keeps the nearing-range context around the hippocampus while reducing the computation burden, it abandons most of the long-range dependent spatial information in the whole brain structure, which bounds the segmentation performance. What's worse, the empirically cropping operation does not guarantee for dealing with the data error caused by medical instrument malfunction, and we have to adapted the crop localization according to different objects which is quietly inconvenient in practice. To introduce the holistic view of the original input data, we need to incorporate the previously inferred enhancement mask \mathbf{M} that contains the holistic information with the original data as follows:

$$\mathbf{X}' = \mathbf{M} \odot \mathbf{C}_{original}, \quad (4)$$

where \mathbf{X}' ($\mathbf{X}' \in \mathbb{R}^{w \times h \times d}$) is the enhanced input data that will be fed into the segmentation network and \odot denotes the dot-product operator.

Then we crop a volume with the size of $h \times w \times d$ that covers the target region and centering at \mathbf{V}_{center} .

Given the estimated location of the hippocampus, we also need to incorporate the holistic information to the cropped data before feeding into the segmentation network. We denote the cropped $h \times w \times d$ volume centered at \mathbf{v}_{center} of the

probability map $\mathcal{F}(\mathbf{X})$ as $\mathbf{C}_{proposal} = Crop(\mathcal{F}(\mathbf{X}), \mathbf{v}_{center})$. We also crop a volume from the exact same region of the original input 3D data \mathbf{X} , which is denoted as $\mathbf{C}_{original} = Crop(\mathbf{X}, \mathbf{v}_{center})$.

On one hand, the proposal serves as the attention mask to enhance the likely regions of the hippocampus localization to guide the segmentation. On the other hand, adding bias to the proposal prevent from the information loss, since it does not completely depress the regions with low responses in proposal. Intuitively, the proposal with low responses may still be part of the hippocampus. The experiments show that the proposal-enhanced data actually boosts the estimation accuracy and speeds up the convergence rate of training the fully convolutional neural network.

At the end, the enhanced input \mathbf{X}' is fed into another network that has the same architecture as the proposal network, to create the fine segmentation result.

C. Training Loss

The network is trained by *Dice Loss*. The variable Dice Loss D between two binary segmentation volumes P and G is the same as [1], written as

$$D(P, G) = \frac{2 \sum_{i=1}^N p_i g_i}{\sum_{i=1}^N p_i^2 + \sum_{i=1}^N g_i^2} \quad (5)$$

where the sums run over the N voxels, of the predicted binary segmentation volume $p_i \in P$ and the ground truth binary volume $g_i \in G$.

III. EXPERIMENTAL RESULTS

A. Datasets

Described in this section are several experiments conducted to evaluate the performance of our method for campus segmentation using the publicly available ADNI database¹. The size of the voxels of the image is $1 \times 1 \times 1mm^3$. Each image consists of several slices with the resolution of 256×256 (pixels) and the numbers of slices range from 166 to 256. We utilized 110 normal control subjects, and downloaded their baseline T1-weighted whole brain MRI images along with their hippocampus masks. We train our network as ten-fold cross validation.

B. Implementation details

Proposal Network has the identical structure and parameter settings as *Segmentation Network* despite the different input image size. Each convolution and de-convolution layer has a $3 \times 3 \times 3$ kernel size, and each down and up sampling convolution layer has a $2 \times 2 \times 2$ kernel size. At each block of convolutional layer, the output size is half down and the output channel is double. At each block of de-convolutional layer, the output size is double and the output channel is half down on the contrary. The input data of *Proposal Network* is

¹<http://adni.loni.usc.edu/>

the resized image, while the other is cropped-masked image. The different weight α and bias β will cause significantly different performance for segmentation network. Empirically, we set β as 1 which means the original data will not be suppressed or impressed by β . In other words, dot production with the mask ranging from zero to one will degrade the data. Our mask will preserve the original object details. The value of α determines the influence of the mask which gained from the proposal network. As for that the output of the proposal network is not good enough, the value of α should be well designed. In order to explore the optimal weight, we compare different weights in Sec. III-D.

C. Evaluations Metric

To quantitatively evaluate the proposed method, four metrics were used for performance evaluation. The degree of overlap was measured for two ROIs V_s and V_g , where V_s and V_g are the sets of object(hippocampus) voxels automatically segmented by the segmentation method and manually segmented by clinical expert, respectively.

- **Dice similarity coefficient (DSC)** is a comprehensive similarity metric that measures the degree of overlap of two ROIs

$$DSC = 2 \times \frac{|V_s \cap V_g|}{|V_s| + |V_g|}$$

where $|\cdot|$ is the cardinality of a set.

- **Jaccard similarity coefficient (JSC)**, which is a statistic used for comparing the similarity and diversity of two ROIs, is described as follows:

$$JSC = \frac{|V_s \cap V_g|}{|V_s \cup V_g|} = \frac{|V_s \cap V_g|}{|V_s| + |V_g| - |V_s \cup V_g|}$$

- **Precision Index (PI)** is the ratio between the overlap of two ROIs and the ROI manually segmented by clinical expert, as follows:

$$PI = \frac{|V_s \cap V_g|}{|V_g|}$$

- **Recall Index (RI)** is the ratio between the overlap of two ROIs and the ROI segmented by the segmentation method, as follows:

$$RI = \frac{|V_s \cap V_g|}{|V_s|}$$

A larger value of all the metric mentioned above indicate a better segmentation performance.

D. Selecting weights for enhancement mask

To select optimal value of weights for the mask, we need to analyze the effects of the weight α in training and testing in the first place.

To do so, we assign different values to α , i.e., 0, 0.1, 0.3, 1.0. We first evaluate how the weight influences the training process. We illustrate the training loss (i.e. Dice

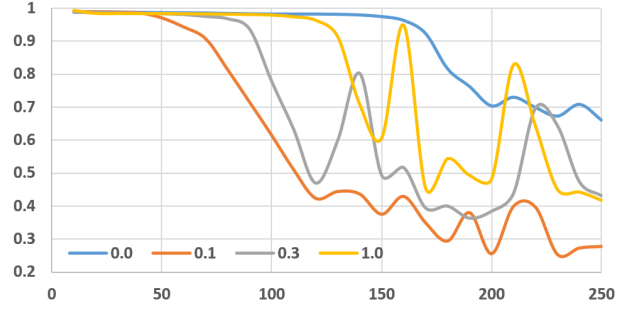


Fig. 2

WE ILLUSTRATE THE TRAINING LOSS(DICE LOSS) OF OUR MODEL WITH VARIED MASK WEIGHTS, I.E., $\alpha = \{0.0, 0.1, 0.3, 1.0\}$, FOR THE FIRST 250 ITERATIONS.

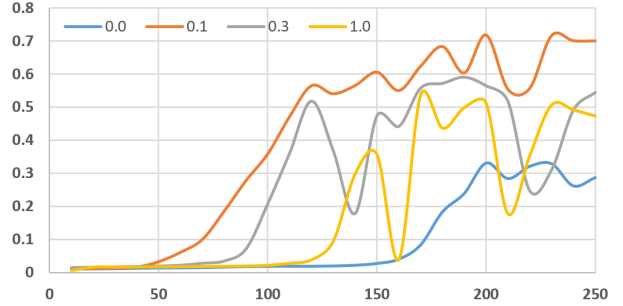


Fig. 3

WE ILLUSTRATE THE TESTING DSC OF OUR MODEL WITH VARIED MASK WEIGHTS, I.E., $\alpha = \{0.0, 0.1, 0.3, 1.0\}$, FOR THE FIRST 250 ITERATIONS.

Loss) in the first 250 epochs with different values of α . According to Fig. 2, as $\alpha = 0.1$, the training loss drops quickly. With $\alpha = 0.3$ and 1.0, the loss also decreases quickly but their curves are not stable. Comparably, without mask (i.e. $\alpha = 0$), the training appears to be slow. It indicates that using the enhancement mask will easily speed up the training, but it may also have the chance to make the training unstable. Besides, we also evaluate the same models with different α in the validation dataset. Their performance is measured using DSC as shown in Fig. 3. Similar to the observation above, the model with $\alpha = 0.1$ has the optimal performance in testing. With $\alpha = 0.3$ and 1.0, the DSC curves are unstable. To sum up, α lets the mask have more impact on the input data, which speeds up the training and enhance the performance of the model. However, too large weights may also cause the overfitting of the trained models. Among these weights, $\alpha = 0.1$ allows the mask to shed some light on the segmentation without jeopardizing the training model. Hence, in the following experiments, we choose $\alpha = 0.1$ as the weight of the enhancement mask.

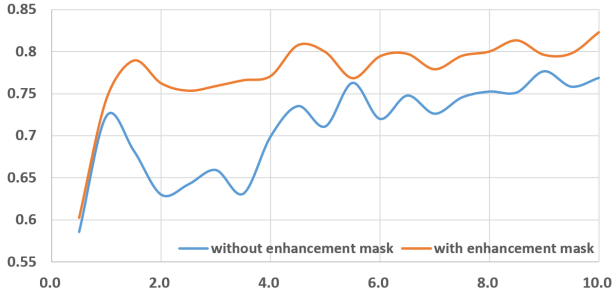


Fig. 4

COMPARISON BETWEEN $\alpha = 0.0$ (WITHOUT MASK) AND $\alpha = 0.1$ AFTER TRAINING FOR $10K$ ITERATIONS.

E. Ablation study

To demonstrate the effect of the mask, we perform comprehensive experiments. First, as shown in Fig. 4, we compare the DSC for the models with and without enhancement mask after training for 10,000 iterations and evaluate their segmentation performance every 500 iterations in the validation dataset. It illustrates that the model with mask achieves significantly better performance after long-term training. Second, as shown in Tab. I, we train the proposal network with iterations ranging from 500 to 5,500, respectively. They are denoted as $N_{pr}^{0.5}, N_{pr}^{1.0}, \dots, N_{pr}^{5.5}$. Similarly, we train the segmentation network with different numbers of iterations as well. They are denoted as $N_{seg}^{0.0}, N_{seg}^{0.5}, \dots, N_{seg}^{5.0}$. Generally, the performance of networks gets better after more training epochs, e.g., $N_{pr}^{2.5}$ is better than $N_{pr}^{2.0}$, and $N_{seg}^{4.0}$ is worse than $N_{seg}^{5.0}$. We pair each proposal network, N_{pr}^i , with a segmentation network, N_{seg}^j , to form a variant of our model. We evaluate these variants to analyze how the proposal network and the segmentation network affect each other. Observing columns in Tab. I, using better proposal network with the same segmentation network may lead to a boost of the performance, especially combining with better segmentation network. It turns out the proposal indeed makes contributions in the segmentation. Another fact is that the model can achieve satisfactory performance without fully trained proposal network. For instance, after training the proposal network for only 1500 epochs, the model can reach more than 0.86 accuracy in DSC that is comparable to the state-of-the-art approaches. This is another benefit of the enhancement mask, which give our confidence for reducing the training iterations of *Proposal Network* to less than 1000. Finally, we evaluate the proposal network with the segmentation networks with and without mask in the validation dataset. As we observe in Fig. 5, the proposal network has only 0.810 accuracy in DSC and the segmentation network without mask gain 0.863. The model with the enhancement mask performs better than them with 0.897. As an example shown in Fig. 6,

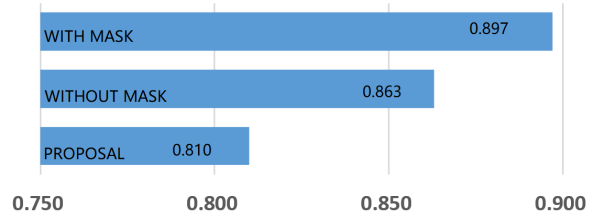


Fig. 5

COMPARISON OF *proposal network*, *segmentation network without enhancement mask* AND *segmentation network with enhancement mask* (DSC).

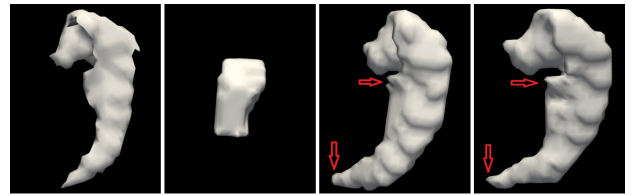


Fig. 6

HIPPOCAMPAL DETECTION AND SEGMENTATION RESULTS BY OUR METHOD. **FIRST:** THE MANUAL SEGMENTATION HIPPOCAMPAL STRUCTURE. **SECOND:** THE RESULTS OF OUR *Proposal Network*. **THIRD:** THE SEGMENTATION OF THE HIPPOCAMPAL STRUCTURE WITHOUT ENHANCEMENT MASK. **FOURTH:** THE SEGMENTATION OF THE HIPPOCAMPAL STRUCTURE WITH ENHANCEMENT MASK.

the top-left figure shows the manual labeled hippocampus. The top-right figure shows the output proposal of the proposal network with the original resolution. It correctly localizes the hippocampus, but it is difficult to discriminate the structural details. The bottom two figures visualize the hippocampus segmentation with and without mask. As illustrated in the area pointed by the red arrow, the result generated by the model with mask has fewer artifacts and more accurate segmentation in the tail of the hippocampus.

F. Quantitative comparison

In this experiment, we adopt 10-fold cross-validation strategy to evaluate the segmentation of the left and the right hippocampus respectively. For comparison purposes, the conventional patch-based method by non-local weighting (Nonlocal-PBM) [14], the recently proposed sparse patch-based labeling (Sparse-PBM) [15] and Path-Based Label Fusion (PBLF) [16] are evaluated on the samples collected on ADNI dataset.

We compare the proposed model with these methods and evaluate on four metrics as shown in Tab. II. According to the quantitative comparison, our approach generally outperforms

TABLE I

COMBINATION OF *Proposal Network* AND *Segmentation Network* TRAINED WITH DIFFERENT NUMBERS OF ITERATIONS. THE *0.0 K Iter.* IN THE FIRST COLUMN INDICATES THE ORIGINAL SEGMENTATION DSC OF *Proposal Network*.

Iteration (K)	0.0	0.5	1.0	1.5	2.0	2.5	3.0	3.5	4.0	4.5	5.0
0.5	0.5856	0.6299	0.7458	0.7726	0.7570	0.7510	0.7498	0.7550	0.7596	0.7861	0.7796
1.0	0.7232	0.7397	0.8248	0.8408	0.8363	0.8406	0.8433	0.8457	0.8473	0.8540	0.8543
1.5	0.6818	0.7529	0.8377	0.8534	0.8487	0.8498	0.8562	0.8560	0.8573	0.8649	0.8664
2.0	0.6297	0.7596	0.8407	0.8538	0.8500	0.8514	0.8559	0.8562	0.8580	0.8645	0.8655
2.5	0.6421	0.7515	0.8366	0.8516	0.8456	0.8458	0.8525	0.8535	0.8551	0.8631	0.8629
3.0	0.6590	0.7516	0.8356	0.8523	0.8464	0.8462	0.8531	0.8530	0.8551	0.8636	0.8633
3.5	0.6308	0.7612	0.8413	0.8546	0.8516	0.8520	0.8571	0.8573	0.8588	0.8652	0.8652
4.0	0.6988	0.7504	0.8339	0.8478	0.8439	0.8464	0.8518	0.8520	0.8537	0.8618	0.8607
4.5	0.7349	0.7578	0.8408	0.8563	0.8533	0.8547	0.8589	0.8607	0.8617	0.8674	0.8687
5.0	0.7107	0.7542	0.8372	0.8518	0.8489	0.8500	0.8548	0.8549	0.8573	0.8643	0.8637
5.5	0.7625	0.7648	0.8472	0.8610	0.8595	0.8607	0.8647	0.8659	0.8659	0.8708	0.8728

TABLE II

COMPARISON WITH OTHER METHODS ON THE LEFT AND RIGHT HIPPOCAMPUS SEGMENTATION.

	DSC	JSC	PI	RI
NLP [14]	0.848/0.865	0.752/0.764	0.878/0.883	0.857/0.864
SPL [15]	0.868/0.880	0.763/0.778	0.887/0.878	0.866/0.875
PBLF [16]	0.879/0.889	0.773/0.789	0.903/0.914	0.879/ 0.889
Ours	0.897/0.900	0.798/0.813	0.892/ 0.919	0.904/0.882

other methods with the obvious advantages in the metrics DSC and JSC.

IV. CONCLUSION AND FUTURE WORK

In this work, we proposed a two-stage hippocampus detection and segmentation framework based on 3D fully convolutional neural network, and we further improve the segmentation performance by introducing an enhancement mask. Our experiments demonstrate that the enhancement mask generated from *Proposal Network* speeds up the convergence of the training process and achieves significant improvements by concatenating with *Segmentation Network*. Furthermore, our model can be easily extended to other biological tissue or organ detection and segmentation problems. As the future work, the two-stage neural network can be upgraded to an end-to-end trainable model, and the optimal value of parameters α and β can also be learned from data.

REFERENCES

- [1] F. Milletari, N. Navab, and S. A. Ahmadi, "V-net: Fully convolutional neural networks for volumetric medical image segmentation," in *Fourth International Conference on 3d Vision*, 2016.
- [2] S. Doyle, A. Madabhushi, M. Feldman, and J. Tomaszewski, "A boosting cascade for automated detection of prostate cancer from digitized histology," in *International Conference on Medical Image Computing and Computer-Assisted Intervention*, 2006.
- [3] K. Nguyen, A. Sarkar, and A. K. Jain, "Structure and context in prostatic gland segmentation and classification," 2012.
- [4] A. Tabesh, M. Teverovskiy, H. Y. Pang, V. P. Kumar, D. Verbel, A. Kotsianti, and O. Saidi, "Multifeature prostate cancer diagnosis and gleason grading of histological images," *IEEE Transactions on Medical Imaging*, 2007.
- [5] K. Sirinukunwattana and N. M. Rajpoot, "A novel texture descriptor for detection of glandular structures in colon histology images," in *Medical Imaging 2015: Digital Pathology*, 2015.
- [6] D. Altunbay, C. Cigir, C. Sokmensuer, and C. Gunduzdemir, "Color graphs for automated cancer diagnosis and grading," *IEEE Transactions on Biomedical Engineering*, 2010.
- [7] C. Gunduz-Demir, M. Kandemir, A. B. Tosun, and C. Sokmensuer, "Automatic segmentation of colon glands using object-graphs," *Medical Image Analysis*, 2010.
- [8] H. Fu, G. Qiu, J. Shu, and M. Ilyas, "A novel polar space random field model for the detection of glandular structures," *IEEE Transactions on Medical Imaging*, 2014.
- [9] K. Sirinukunwattana, D. Snead, and N. Rajpoot, "A stochastic polygons model for glandular structures in colon histology images," *IEEE Transactions on Medical Imaging*, 2015.
- [10] J. Long, E. Shelhamer, and T. Darrell, "Fully convolutional networks for semantic segmentation," *IEEE Transactions on Pattern Analysis and Machine Intelligence*, 2017.
- [11] H. Noh, S. Hong, and B. Han, "Learning deconvolution network for semantic segmentation," in *IEEE International Conference on Computer Vision*, 2015.
- [12] O. Ronneberger, "Invited talk: U-net convolutional networks for biomedical image segmentation," 2017.
- [13] O. Cicek, A. Abdulkadir, S. S. Lienkamp, T. Brox, and O. Ronneberger, "3d u-net: Learning dense volumetric segmentation from sparse annotation," 2016.
- [14] P. Coup, J. V. Manjn, V. Fonov, J. Pruessner, M. Robles, and D. L. Collins, "Nonlocal patch-based label fusion for hippocampus segmentation," *Med Image Comput Comput Assist Interv*, 2010.
- [15] D. Zhang, Q. Guo, G. Wu, and D. Shen, "Sparse patch-based label fusion for multi-atlas segmentation," in *International Workshop on Multimodal Brain Image Analysis*, 2012.
- [16] Y. Wang, G. Ma, X. Wu, and J. Zhou, "Patch-based label fusion with structured discriminant embedding for hippocampus segmentation," *Neuroinformatics*, 2018.